ARCHITECTURE. CONSTRUCTION
Vol. 2 | №1 | 2025
ISSN 1694-8866
Journal homepage:
https://arch-constr-journal.com/en

UDC 624.131.3:624.131.5:004.94
DOI: 10.63621/as./1.2025.09

Study on the application of dynamic compaction reinforcement at the cut-and-fill interface of high-fill foundation slopes at an airport

Cheng Xiaobing*
Postgraduate Student
Vinnytsia National Technical University
21021, 95 Khmelnytske Shosse Str., Vinnytsia, Ukraine
Master
Jiuquan Vocational and Technical University
735000, 66 Jiefang Road., JiuQuan, China
https://orcid.org/0009-0002-9675-6410

Viacheslav Dzhedzhula
Doctor of Economic Sciences, Professor
Vinnytsia National Technical University
21021, 95 Khmelnytske Shosse Str., Vinnytsia, Ukraine
https://orcid.org/0000-0002-2740-0771

Abstract. Due to the strict protection of arable land in China, an increasing number of high-fill projects involving "mountain excavation and ditch filling" have emerged. Improper treatment of the cut-and-fill interface may lead to engineering failures, such as differential settlement and slope instability. This article aimed to reveal the mechanism of dynamic compaction on fill soils and the impact of variations in the water environment on compaction effectiveness, thereby formulating scientifically grounded engineering strategies to address the issue of weak interfaces in cut-and-fill zones. Based on a high-fill airport project in a mountainous region of northwest China, a series of dynamic compaction tests with varying energy levels, static load immersion tests on the original foundation soil, and laboratory geotechnical experiments were conducted. The safety factor of the reinforced slopes was evaluated using the FLAC3D numerical model. The findings indicated that settlement from a single tamping action increased with greater energy input and decreased with the number of tamping cycles. The greatest settlement occurred during the initial 3-4 tamping passes and gradually stabilised after 6-8 passes. Following compaction, both the dry density and compressive modulus of the soil increased; the degree of improvement was positively correlated with tamping energy and gradually diminished with increased sampling depth. The results of the static load immersion test in the direct current area demonstrated that water immersion led to additional settlement of compacted soil. However, higher tamping energy during compaction resulted in less post-immersion settlement. These outcomes provide a theoretical foundation for designing direct current parameters and implementing engineering measures to mitigate soft zone issues at the cut and-fill interface

Keywords: mountain engineering; static load immersion test; weak layer reinforcement; interface strengthening method; FLAC3D numerical simulation

Introduction

With the rapid development of China's air transportation industry, the scale of airport construction has been expanding. Under the strict constraints of the "1.8 billion mu of arable land" red line, which must not be infringed, high-fill slope engineering has been increasingly adopted in mountainous, hilly, and other complex

Suggested Citation: Xiaobing, C., & Dzhedzhula, V. (2025). Study on the application of dynamic compaction reinforcement at the cut-and-fill interface of high-fill foundation slopes at an airport. *Architecture. Construction*, 2(1), 9-21. doi: 10.63621/as./1.2025.09.

*Corresponding author

terrain conditions. As the transition zone between the fill and the original foundation, the cut-and-fill interface is highly susceptible to forming weak zones, which may lead to engineering issues such as differential settlement, interface slippage, and even slope instability. Therefore, enhancing the overall stability of the cut-and-fill interface through scientific and effective reinforcement techniques has become a central challenge in the construction of high-fill airports in mountainous regions. However, research on the mechanism of direct current (DC) reinforcement for the complex cut-and-fill interface system remains limited.

In response to these challenges, numerous scholars have conducted extensive research on the application of DC.L. Wang *et al.* (2023) carried out a field-based DC test and found that the impact energy of DC fluctuated significantly at the interface between soft and hard soil layers. They recommended using low-energy, closely spaced, multi-layer ramming for reinforcement near the interface. However, the study did not specify the energy levels or the number of blows required to achieve the desired compaction effect. P. Li *et al.* (2023) performed a series of field DC tests, treating energy level, hammer mass, and hammer diameter as variables, and recorded vibration attenuation waveforms at various soil locations during the DC process. Their results showed that, at the same energy level, "heavy hammer, low blow" methods provided better reinforcement and reduced ground vibrations compared to "light hammer, high blow" techniques. However, the influence of the cutandfill interface on the overall reinforcement effect was not considered in their study. Based on the FDM-DEM approach, Y. Sun *et al.* (2023) conducted three-dimensional fluid-solid coupling numerical simulations of DC and revealed that vertical additional dynamic stresses are the primary drivers of foundation compaction. They found that a compaction energy level of 8,000 kN · m resulted in a maximum effective reinforcement depth of 11 metres. However, this study did not account for the influence of soil type parameters. L. Xi *et al.* (2020) proposed an optimisation model for DC parameters based on energy transfer efficiency using PFC3D simulations. Additionally, W.H. Zhou *et al.* (2022), through discrete element method simulations, discovered that matching the bottom area of the DC hammer with the stiffness of the soil could reduce the risk of interfacial slip. Based on field and laboratory tests, W. Ni *et al.* (2024) investigated the mechanical behaviour and microstructural evolution of Malan loess under DC conditions. S. Wu *et al.* (2020) analysed the mechanism behind the strength enhancement of soil-rock mixtures due to compaction energy in airport filling projects, summarised the relationship between compaction and vibration velocity, and proposed the concept and method for determining the critical elastic vibration velocity of soil-rock mixtures. Z. Yao *et al.* (2022) studied the effect of multi-point ramming during DC on the density of sandy soil between adjacent impact points using numerical modelling. Y. Mei *et al.* (2021) observed that DC reinforcement with energy levels exceeding 2,000 kN · m can effectively improve the foundation of deep wetted loess. J. Zhu *et al.* (2025) explored the influence of ramming parameters on vibration velocity during DC in heterogeneous fill sites using back-propagation (BP) neural network modelling. M. Jia *et al.* (2021a) quantified the correlation between DC parameters and pore water pressure through model testing, focusing on the dynamic changes in pore water pressure generated during DC (including peak characteristics and dissipation behaviour). Under low water level conditions, the peak value of excess pore water pressure increased significantly with the number of DC applications, while shallow pore water pressure took longer to dissipate due to the direct modelling test conditions. However, none of these studies considered the effect of differences in permeability at the interface between powdery clay and gravel. The present study aimed to develop a reinforcement method for the interface between backfill and powdery clay layers to ensure the safety and stability of slopes.

Materials and Methods

To address the limitations of existing research – such as the incomplete consideration of influencing factors, inconsistencies in ramming termination criteria, and the lack of attention to the differences between soil layers at the cut-and-fill interface – this study focused on a 60-metre-high fill slope at an airport in northwest China. The relationship between the number of blows and the magnitude of ramming-induced settlement was analysed to establish a standard for terminating ramming. Additionally, the impact of changes in water conditions on the effectiveness of DC was investigated.

The test site is a regional airport in northwest China, categorised as flight area index 4C, with a runway length of 2,800 m and a total width of 48 m (including a 45 m-wide pavement and 1.5 mwide shoulders on both sides). The site extends approximately 3,800 m in length and 450 m in width, covering an area of about 1.71 million m^2. The topography consists of low hills with significant variations in elevation and the presence of erosion gullies, two of which – running north to south – cross the entire field. Ground elevation ranges from 1,067 to 1,181 m, with a relative height difference of 114 m. Large-scale earthworks, including both excavation and filling, are required, with 15 fill slopes exceeding 20 m in height. The tallest, filling slope No. 1, has a height difference of approximately 60 m between its crest and base. Considering the actual topographical and geological conditions, the largest filling area – comprising both the road and slope sections – was selected as the test zone. This area, which includes conditions such as soft foundation treatment, fill material optimisation, cut-and-fill interface handling, deep excavation, and high embankment filling, was deemed typical and representative. The geological investigation report indicates the distribution of strata as follows: an arable soil layer (Q4ml, 0.1-2.4 m), a powdery clay layer (Q4dl + pl, 0.2-15.5 m, with a characteristic foundation bearing capacity value of 120 kPa), a strongly weathered sandy mudstone layer (N2, 2.9-5.7 m, 400 kPa), and a moderately weathered sandy mudstone layer (N2, 1.3-46.9 m, 500 kPa).

According to the zoning classification based on differing engineering geological conditions, the runway excavation and fill interface is designated as Area 1, the filling zone of Slope No. 1 as Area 2, and the excavation zone as Area 3. The arable soil layer was removed during surface clearing and is therefore not considered in this study. The average values of the main physical and mechanical properties of the powdery clay layer are presented in Table 1.

Table 1. Main physical and mechanical properties of the powdery clay layer

Property	Area 1	Area 2	Area 3
Density ρ/(g·cm^{-3})	1.86	1.8	1.83
Moisture content w/%	19.4	19.15	18.87
Plastic limit w_p/%	21.91	21.69	22.87
Liquid limit w_l/%	32.66	32.4	34.84
Porosity ratio e	0.76	0.82	0.79
Cohesion c/kPa	35		
Angle of internal friction ϕ/°	22		
Coefficient of compressibility α_{1-2}/MPa^{-1}	0.16	0.2	0.25
Modulus of compressibility E_s/MPa	11	8.6	7.1

Source: measured by the authors at the construction site

The indicators in Table 1 were obtained from samples taken at the site. The soil exhibits low density and compressibility modulus, and as it lies at the cut-and-fill interface, compaction is required during construction to enhance its bearing capacity. Located beneath the powdery clay layer were the strongly weathered and moderately weathered mudstone layers. The average values of their main physical and mechanical properties are provided in Table 2.

Table 2. Main physical and mechanical properties of the bedrock layers

Property	Strongly weathered mudstone			Moderately weathered mudstone		
	Area 1	Area 2	Area 3	Area 1	Area 2	Area 3
Density ρ/(g·cm^{-3})	2.09	2.08	2.05	2.15	2.14	2.1
Moisture content w/%	14.99	13.8	11.34	14.29	13.21	10.72
Cohesion c/kPa	55			95		
Angle of internal friction ϕ/°	0.14	0.15	0.14	5.62	5.97	5.55
Elastic modulus E/MPa	250	247.1	239.9	773	762.1	757.1
Poisson ν	0.33	0.33	0.32	0.31	0.3	0.3

Source: measured by the authors

Table 2 summarises the key parameters of the strongly and moderately weathered mudstone layers in various areas of the airport. These layers exhibit high density, cohesion, and elastic modulus. According to the geological investigation report, the characteristic foundation-bearing capacities of these layers were 400 kPa and 500 kPa, respectively. To determine the optimum DC parameters, field dynamic compaction tests were carried out in the powdery clay layer at the western end of the runway using four energy levels: 1,000, 2,000, 3,000, and 4,000 kN · m. Each energy level was divided into two test zones. Construction parameters are detailed in Table 3. With the exception of the 1,000 kN · m energy level, each test area was initially tamped twice using a quincunx grid arrangement, followed by one complete DC pass after levelling, employing 1,000 kN · m energy with point spacing equivalent to one-third of the hammer mark overlap. The rammer used in the tests had a base diameter of 2.5 m, resulting in a contact area of 4.9 m². During the DC process, average settlement values due to tamping were recorded. Upon completion of the tests, reinforcement effects were evaluated both at the centre of the tamping points and in the interstitial areas between compaction points.

Table 3. Construction parameters for each test area

DC level (kN · m)	Test area	Compaction spacing /m	Rammer weight /T	Rammer drop height/m
1,000	A1-1	3.0	23.6	4.3
	A1-2	1/3 overlap of hammer marks	23.6	4.3
2,000	A2-1	3.5	23.6	8.5
	A2-2	4.0	23.6	8.5

Table 3. Continued

DC level (kN·m)	Test area	Compaction spacing /m	Rammer weight /T	Rammer drop height/m
3,000	A3-1	4.0	23.6	12.7
	A3-2	4.5	23.6	12.7
4,000	A4-1	4.0	23.9	16.7
	A4-2	4.5	23.9	16.7

Source: measured by the authors

Table 3 presents the four DC energy levels along with their corresponding compaction point spacing, rammer mass, and drop height. These configurations were primarily designed to investigate the dynamic response of compacted soil under different parameter conditions, thereby providing data to support the optimisation of DC parameters in practical construction.

Due to the high moisture content of the original powdery clay layer in the test area, and recognising that soil strength recovery requires a certain period after DC treatment, exploratory pits were excavated in each test section two weeks after compaction. These pits allowed for the collection of in situ soil samples at varying depths to ensure that subsequent laboratory analyses accurately reflected the post-treatment condition of the soil. Laboratory geotechnical testing was conducted following the Standard for Geotechnical Test Methods (GB/T 50123-2019, 2019). These tests were used to determine the average dry density (ρ_d), compaction coefficient (η), and compression modulus (E_s) of the foundation soil before and after dynamic compaction.

To evaluate the bearing capacity and stability of the DC-treated foundation soil, and to assess additional settlement under altered hydrological conditions, three parallel static load immersion tests were conducted in test areas A2-1, A3-1, and A4-1. A circular bearing plate with a diameter of 0.8 m was used, and test pits were excavated to dimensions of 2.4 m in diameter and 0.7 m in depth. Following the Standard for Building Construction in Collapsible Loess Regions (GB 500252018, 2018), the testing procedure was as follows: initial dry loading was applied under static load immersion conditions; graded loading was carried out until stabilisation at 600 kPa; unloading proceeded to 300 kPa; water was then introduced into the test pits to induce additional settlement. Once this additional settlement had stabilised, unloading continued in graded steps. Settlement was recorded at each stage of loading, unloading, and immersion throughout the test.

Results and Discussion

Upon completion of the tests, two sets of relationship curves were plotted: settlement versus the number of tamping passes for each test area (Fig. 1). These curves were derived from single-pass settlement measurements and cumulative settlement data.

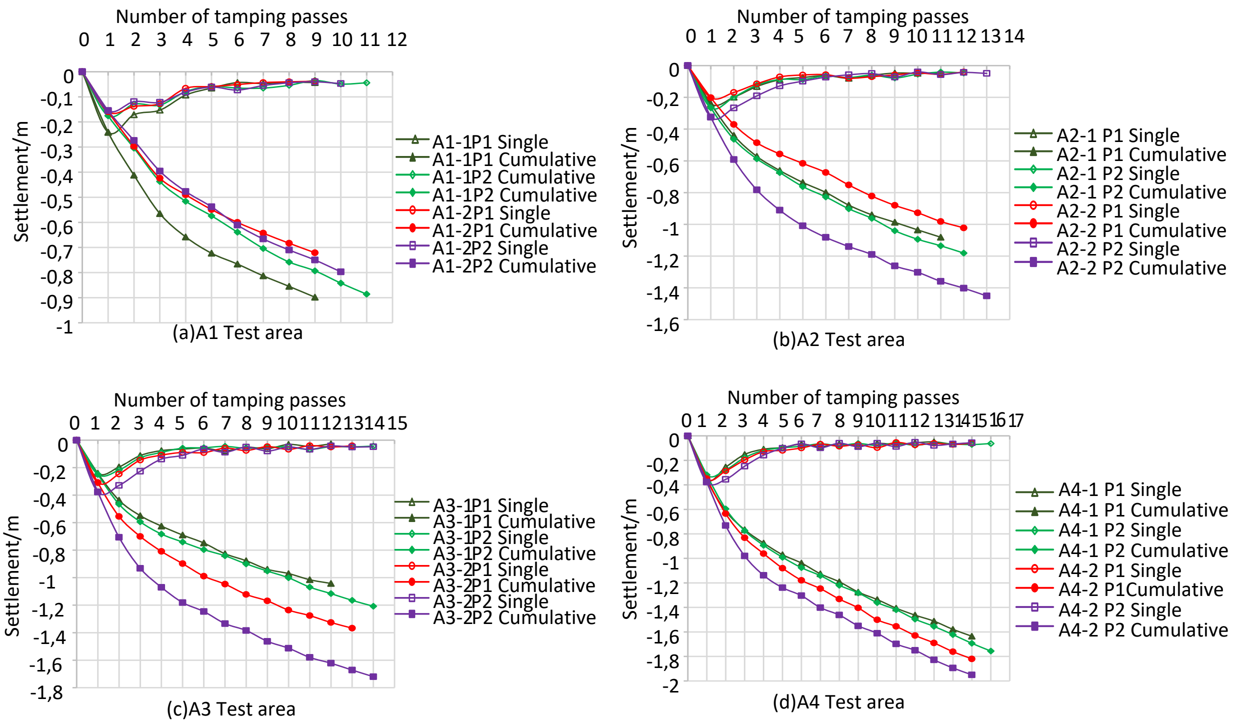

Figure 1. Relationship curves of settlement versus the number of tamping passes for each test area
Source: compiled by the authors

As shown in Figure 1, cumulative settlement in each test area increased with the number of tamping passes. During the initial 3-4 passes (particularly the first three), the single-pass settlement was significantly larger, ranging from 0.1 to 0.3 m per tamping cycle. The cumulative settlement exhibited a steep increasing trend during this phase. Beyond the 6^{th}-8^{th} passes, the single-pass settlement gradually decreased, though cumulative settlement continued to rise. After the 10^{th} pass, single-pass settlement declined markedly, and the cumulative settlement curve began to converge with the tamping pass count. The test tamping results for each test area are summarised in Table 4.

Table 4. Tamping test results for each test area

DC level (kN·m)	Test area	Number of tamping passes	Cumulative settlement /m	Average settlement of the final three passes /cm	Termination criterion /cm
1,000	A1-1	9-11	0.86-0.89	4.3-4.6	4.5
	A1-2	9-10	0.72-0.84	4.0-4.3	
2,000	A2-1	11-12	1.08-1.18	4.7	5
	A2-2	12-13	1.02-1.45	4.7-5.7	
3,000	A3-1	12-14	1.04-1.20	3.3-4.7	5
	A3-2	13-14	1.33-1.72	4.3-4.7	
4,000	A4-1	15-16	1.63-1.80	5.7-6.7	7
	A4-2	15	1.82-1.95	6.4-6.7	

Source: data obtained by the authors

Analysis of Table 4 reveals that higher dynamic compaction energy levels required more tamping passes to achieve stabilisation and resulted in greater cumulative settlement. During the tests, a slight heave (approximately 6-11 cm) was observed in the shallow soil surrounding the tamping pits, indicating that the hammer's impact energy was predominantly transferred to the underlying foundation soil. The optimal number of tamping passes for the 2,000 kN·m, 3,000 kN·m, and 4,000 kN·m energy levels was determined to be 11-12, 12-14, and 15-16 passes, respectively. Based on the average settlement of the final three passes, the termination criteria for the four energy levels were defined as settlements not exceeding 4.5 cm, 5 cm, 5 cm, and 7 cm, respectively.

Additionally, for a given energy level, cumulative settlement increased with larger tamping point spacing, and more passes were required to meet the termination criteria. Furthermore, the influence of tamping point spacing on the cumulative settlement was less significant than that of the energy level, demonstrating that energy level predominantly governed the effectiveness of DC on the original foundation soil and should be prioritised as the key design parameter. The test results for the average dry density (ρ_d) and compaction coefficient (η) of the foundation soil before and after DC are presented in Table 5. The maximum dry density of the original powdery clay layer was 1.89 g/cm³.

Table 5. Average dry density of soil before and after DC in each test area

Test area		Sampling depth /m							
		1	2	3	4	5	6	7	8
A1-1	Untreated ρ_d /(g/cm³)	1.59	1.54	1.56	1.60	1.55	—	—	—
	Treated ρ_d /(g/cm³)	1.87	1.73	1.69	1.68	1.61	—	—	—
	Increase in ρ_d /%	17.61	12.34	8.33	5.00	3.87	—	—	—
	Untreated η	0.83	0.84	0.85	0.84	0.84	—	—	—
	Treated η	0.96	0.92	0.89	0.87	0.86	—	—	—
	Increase in η /%	15.66	9.52	4.71	3.57	2.38	—	—	—
A2-1	Untreated ρ_d /(g/cm³)	1.58	1.54	1.63	1.58	1.56	1.55	—	—
	Treated ρ_d /(g/cm³)	1.83	1.75	1.78	1.69	1.67	1.62	—	—
	Increase in ρ_d /%	15.82	13.64	9.20	6.96	7.05	4.52	—	—
	Untreated η	0.85	0.82	0.86	0.85	0.84	0.85	—	—
	Treated η	0.99	0.93	0.94	0.91	0.9	0.88	—	—
	Increase in η /%	16.47	13.41	9.30	7.06	7.14	3.53	—	—
A3-1	Untreated ρ_d /(g/cm³)	1.58	1.6	1.62	1.58	1.61	1.6	1.58	—
	Treated ρ_d /(g/cm³)	1.8	1.78	1.79	1.74	1.7	1.7	1.65	—
	Increase in ρ_d /%	13.92	11.25	10.49	10.13	5.59	6.25	4.43	—
	Untreated η	0.85	0.85	0.86	0.84	0.85	0.86	0.85	—
	Treated η	0.97	0.95	0.96	0.92	0.9	0.91	0.88	—
	Increase in η /%	14.12	11.76	11.63	9.52	5.88	5.81	3.53	—
A4-1	Untreated ρ_d /(g/cm³)	1.6	1.61	1.59	1.59	1.61	1.6	1.59	1.61

Table 5. Continued

Test area		Sampling depth /m							
		1	2	3	4	5	6	7	8
A4-1	Treated ρ_d /(g/cm³)	1.79	1.81	1.78	1.71	1.76	1.69	1.71	1.67
	Increase in ρ_d /%	11.88	12.42	11.95	7.55	9.32	5.62	7.55	3.73
	Untreated η	0.85	0.84	0.86	0.84	0.85	0.85	0.85	0.86
	Treated η	0.96	0.95	0.95	0.91	0.92	0.91	0.9	0.89
	Increase in η /%	12.94	13.10	10.47	8.33	8.24	7.06	5.88	3.49

Source: data obtained by the authors

As shown in Table 5, the dry density (ρ_d) of the untreated foundation soil ranged from 1.54 to 1.63 g/cm³. After DC treatment, the dry density (ρ_d) within the tested depth increased to 1.611.87 g/cm³, indicating a significant improvement in soil compaction at specific depth intervals. The extent of improvement decreased progressively with depth, with the maximum increase in compaction coefficient (η) reaching 16.47%. The rate of increase in compaction coefficient (η) diminished with greater sampling depth: 0-2 m depth: 9.52%-16.47% increase; 2-4 m depth: 3.57%-10.47% increase; >4m depth: 2.38%-8.24% increase. The maximum depths at which the compaction coefficient (η) exceeded 0.90 in the four test plots were 2 m, 5 m, 6 m, and 7 m, respectively. Based on the before and after DC test results, relationship curves showing the increase in ρ_d versus sampling depth were plotted for each test area and are presented in Figure 2.

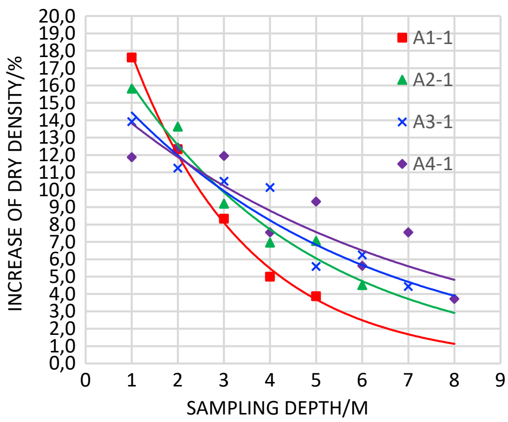

Figure 2. Relationship between the increase in dry density and sampling depth
Source: compiled by the authors

As shown in Figure 2, the increases in dry density across all test areas gradually decreased with sampling depth following DC treatment. Notably, the A1-1 test area exhibited the steepest decline in density enhancement, followed by A2-1 and A3-1, while A4-1 showed the least reduction. This trend corresponds with the applied DC energy levels: A1-1 received the lowest energy input (1,000 kN · m), whereas A4-1 received the highest (4,000 kN · m). These results reaffirm the conclusion from the DC tests that energy level exerts a dominant influence on the compaction effectiveness of the original foundation soil and should be prioritised as the key design factor. Based on the test results presented in Table 5, relationship curves between the compaction coefficient and sampling depth before and after DC were plotted and are shown in Figure 3.

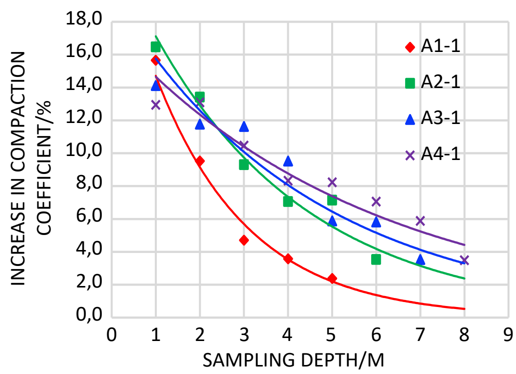

Figure 3. Relationship between the increase in compaction coefficient and sampling depth
Source: compiled by the authors

As seen in Figure 3, the increase in the compaction coefficient decreased with increasing sampling depth. The A1-1, which received the lowest DC energy level, exhibited the greatest reduction in improvement, while A4-1, which received the highest energy level, showed the smallest decrease. This suggests a positive correlation between the depth of effective reinforcement and the DC energy level. The values of the compression modulus (E_s) are detailed in Table 6.

Table 6. Soil compression modulus before and after DC in each test area

Project name		Sampling depth /m							
		1	2	3	4	5	6	7	8
A1-1	Untreated E_s (MPa)	6.1	6.0	6.3	6.1	7.2	—	—	—
	Treated E_s (MPa)	18.7	18.3	15.2	10.1	9.6	—	—	—
	Increase rate /%	206.56	205.00	141.27	65.57	33.33	—	—	—

Table 6. Continued

Project name		Sampling depth /m							
		1	2	3	4	5	6	7	8
A2-1	Untreated E_s (MPa)	7.5	6.2	7.4	7.6	6.3	6.2	—	—
	Treated E_s (MPa)	19.9	16.7	17.3	15.6	10.2	9.7	—	—
	Increase rate /%	165.33	169.35	133.78	105.26	61.90	56.45	—	—
A3-1	Untreated E_s (MPa)	8.2	8.3	10.4	8.5	8.3	8.9	7.8	—
	Treated E_s (MPa)	22.3	17.9	21.6	17.2	15.5	16.5	10.9	—
	Increase Rate /%	171.95	115.66	107.69	102.35	86.75	85.39	39.74	—
A4-1	Untreated E_s (MPa)	7.4	7.5	8.1	8.1	8.2	8.5	7.7	7.6
	Treated E_s (MPa)	20.1	18.3	16.4	18.4	18.7	16.9	13.8	10.2
	Increase rate /%	171.62	144.00	102.47	127.16	128.05	98.82	79.22	34.21

Source: data obtained by the authors

As shown in Table 6, the E_s of the untreated foundation soil ranged from 6.0 to 10.4 MPa. After DC treatment, E_s increased to 9.6-22.3 MPa, indicating a transition from medium-high to mediumlow compressibility. The improvement in E_s was more pronounced in the shallow layers than in the deeper strata. Specifically: at 0-2 m depth, E_s increased by 115.66%-206.56%; at 2-4 m depth, the increase was 65.57%-141.27%; below 4 m depth, the increase ranged from 33.33% to 128.05%. Based on the before and after DC results, relationship curves illustrating the increase in E_s versus sampling depth were plotted for each test area and are shown in Figure 4.

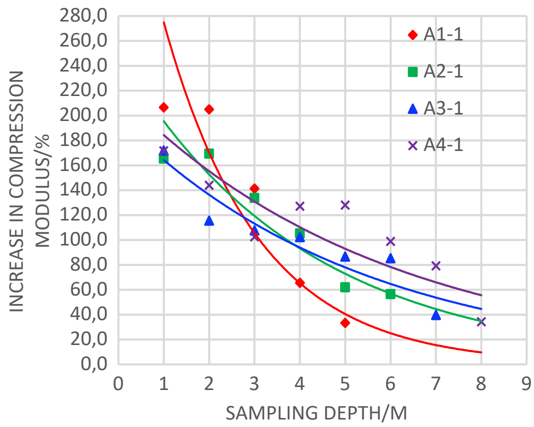

Figure 4. Relationship between the increase in compression modulus and sampling depth
Source: compiled by the authors

As observed in Figure 4, the increase in the soil's compression modulus decreased with greater sampling depth, indicating that DC treatment was more effective in the upper soil layers. Comparing the curves for A1-1 to A4-1, it is evident that increased DC energy levels reduce the sensitivity of E_s improvement to sampling depth, due to deeper effective reinforcement zones associated with higher energy input. It is worth noting that at a DC energy level of 4,000 kN · m, the variation in compression modulus improvement across different depths was more dispersed. This suggests that excessively high DC energy levels may damage soil particles, potentially undermining the stability and uniformity of the reinforcement effect when treating powdery clay. The results of the load immersion tests for each DC test area are summarised in Table 7.

Analysing Table 7, it can be seen that total settlement gradually decreased (from 19.69 mm to 14.01 mm) with increasing DC energy levels (from A2-1 to A4-1). This indicates that high-energy level strong tamping (4,000 kN · m) can significantly enhance foundation compactness and reduce compressive deformation. However, the deformation modulus (24 MPa) of A3-1 (3,000 kN · m) is slightly higher than that of A4-1 (23.5 MPa), which may be attributed to localised soil fragmentation caused by the higher energy level (4,000 kN · m), thereby reducing overall stiffness. The largest residual settlement (18.59 mm) after unloading to 300 kPa, which accounts for 94.4% of the total settlement in A2-1, indicates that the soil predominantly underwent plastic deformation, with poor elastic recovery following treatment with the low-energy rammer (2,000 kN · m). To further analyse the response mechanism of DC-treated soils under changing water conditions, the load-settlement (PS) curve was plotted based on the experimental results in Table 7, as shown in Figure 5.

Table 7. Results of the load immersion tests

Test area	A2-1	A3-1	A4-1
Total settlement under maximum load/mm	19.69	15.68	14.01
Settlement after unloading to 300 kPa/mm	18.59	14.81	12.72
Additional settlement after immersion/mm	14.19	14.98	11.49
Foundation Bearing capacity (corresponding to settlement)/mm	7.87	7.15	7.3
Modulus of deformation/MPa	21.8	24	23.5

Note: a shape factor of 0.785 was used for calculating the deformation modulus, and the Poisson's ratio of the soil was taken as 0.3
Source: data obtained by authors

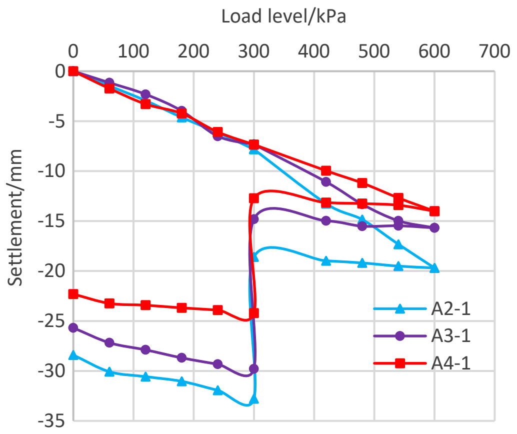

Figure 5. Load-settlement curve from the load immersion test
Source: compiled by the authors

As observed in Figure 5, when the load reached 600 kN, the cumulative settlement ranged from 14.01 to 19.69 mm, and the P-S curves exhibited no distinct inflection points. In accordance with the General Code for Foundation Engineering of Building and Municipal Projects (GB 550032021, 2021), the characteristic value of foundation bearing capacity is defined as the load corresponding to a settlement-to-diameter ratio (s/d) of 0.01-0.015 (360 kPa), but it must not exceed half of the maximum applied load (600 kPa). Therefore, the characteristic bearing capacity was taken as 300 kPa, with corresponding settlements of 7.15-7.87 mm and a deformation modulus of 21.8-24 MPa. Furthermore, under identical loading conditions, soils treated with higher DC energy levels exhibited significantly smaller settlements than those treated with lower energy levels. This further confirms that higher DC energy enhances both bearing capacity and foundation stability.

According to the static load immersion test, additional settlement after immersion stabilisation ranged from 11.19 to 14.98 mm. The ratios of additional settlement to bearing plate diameter at the three test points were 0.0178, 0.0188, and 0.0144, respectively. The first two values exceeded 0.017, satisfying the requirements of the Standard for Building Construction in Collapsible Loess Regions (GB 50025-2018, 2018), but remained below 0.023, as specified in the Code for Investigation of Geotechnical Engineering (GB 50021-2001 (2009), 2002). Comprehensive analysis indicates that the original powdery clay foundation can be classified as a non-wetted collapsible soil layer, provided that overburden pressures do not exceed 300 kPa after qualified DC treatment.

Stability control of high-fill foundations requires attention not only to total settlement and deformation but also to the synergistic deformation mechanisms at the interface between the fill and the original foundation. This consideration is particularly critical when the excavated area has a rocky substrate, as the contact interface is more prone to abrupt changes in stiffness, leading to stress concentrations and differential settlement. Taking the airport project as an example, a thick powdery clay layer was found at the cut-and-fill interface. The investigation results revealed the following:

Wet subsidence characteristics – powdery clay within the −2 to −7 m depth range exhibited Class I non-self-weight collapsibility (with a collapse coefficient $\delta s = 0.015\text{-}0.035$). Submergence was shown to potentially induce additional settlement. Compression characteristics – The compression modulus $Es = 4.2\text{-}6.8$ MPa, indicating moderate to high compressibility, with long-term loading potentially generating further settlement. Interface effects – The stiffness contrast between the fill material (coarse-grained soil) and the original foundation (powdery clay) exceeded a factor of five, creating a potential shear-slip surface. In view of the above engineering challenges, and based on the experimental results of this study, a graded synergistic composite reinforcement method was developed for the junction between excavated and filled areas (Fig. 6).

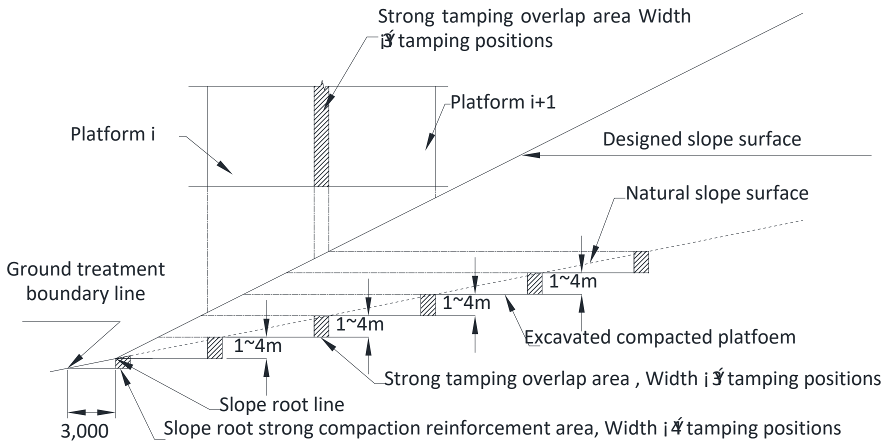

Figure 6. Schematic diagram of the "composite method" for reinforcing the cut-and-fill interface of a high-fill slope
Note: unit – m
Source: compiled by the authors

As shown in Figure 6, the “static transition + dynamic enhancement” method is described as follows: the interface transition layer was optimised by excavating to a depth of 300-600 mm and replacing the material with medium coarse sand or graded gravel bedding. This material’s high permeability accelerated pore water dissipation. The particle size gradation was optimised to achieve a stress diffusion angle of at least 35°, reducing the interface shear stress peak by more than 30%. The thickness of the bedding layer was dynamically designed using the Boussinesq stress distribution theory to ensure that the additional stress attenuated to less than 20% of the original foundation’s bearing capacity characteristic value. In the dynamic reinforcement system, the foot-of-slope reinforcement area was extended 3 m outward from the slope toe line. Here, four rows of dynamic compaction (1,500 kN · m) were applied in a plum blossom pattern, with a spacing of 2.5D (D = 2.4 m), forming a 6 m-deep continuous reinforcement belt to enhance the anti-slip moment. For steep slope stubble treatment, in areas with a natural slope ratio greater than 1:5, reverse steps with a step height of 1-4 m and a minimum width of 2 m were excavated after surface clearing. Three rows of 1,000 kN · m dynamic compaction were applied for every 4 m of fill, eliminating blind zones of impact densification and increasing the interface compaction degree from 87% to 93%. The tamping energy and point density were dynamically adjusted based on real-time settlement monitoring data (with an accuracy of ± 0.1 mm) and shear wave velocity inversion, achieving a *Vs* enhancement rate greater than 15%.

Through this dual mechanism, the composite method controlled differential settlement at the interface within 5 cm per 100 m, significantly reducing post-construction maintenance costs. To verify the effectiveness of the reinforcement, FLAC3D software was used to establish a numerical model, applying the built-in strength reduction method to calculate the post-reinforcement slope safety factor (Dawson *et al*., 2020). As shown in Figure 7, the simulation results indicated that, following treatment, the overall performance at the cut-and-fill interface improved significantly, achieving a slope stability coefficient of *F* = 1.94, which met the project’s design requirements.

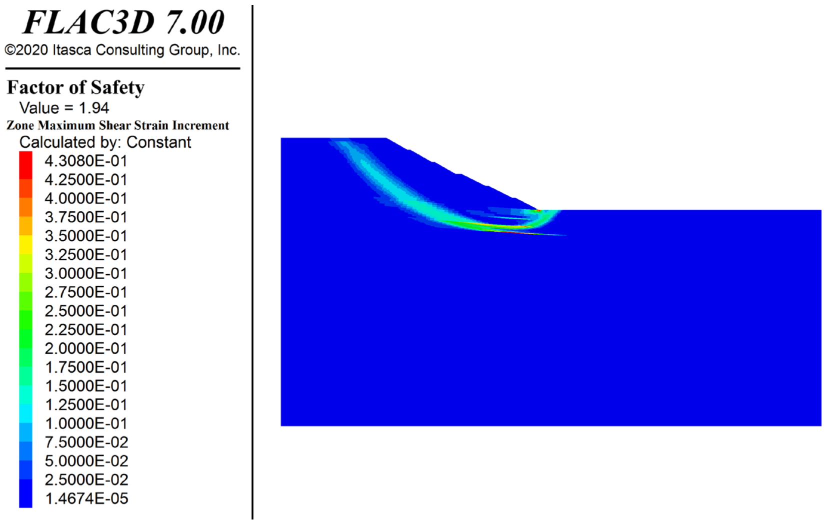

Figure 7. Factor of safety

Source: compiled by the authors

DC, also known as power consolidation, has undergone continual development in both reinforcement mechanisms and application technologies. Researchers have progressively refined the multi-field coupling mechanism, building on the principles of DC, dynamic consolidation, and dynamic replacement. For example, based on field tests and numerical simulations, X. Li *et al*. (2020) introduced the tamping momentum coefficient to evaluate the respective contributions of “hammer weight” and “hammer drop height” to the compaction effect. They found that the contribution of “hammer weight” exceeded that of “hammer drop height” – that is, the energy conversion efficiency of a “heavy hammer with low drop” combination was higher. This configuration reduced surface crust formation and improved the efficiency of deep compaction. In this study, three parameters – “hammer weight”, “hammer drop height” and “tamping point spacing” – were investigated. This approach not only explored the influence mechanism of tamping energy on the compaction effect but also identified the optimal combination of tamping parameters from an engineering application perspective, thereby enhancing the study’s practical relevance. To examine the compaction mechanism of DC on porous bonded residual soil, N.C. Consoli *et al*. (2020) compared the changes in Young’s modulus and the angle of internal friction before and after DC treatment. In contrast, this study further evaluated reinforcement effectiveness by comparatively analysing changes in dry density, compaction coefficient, and compression modulus before and after DC treatment.

L. Zhang *et al.* (2019a) noted that tamping energy should not be excessively high and must be selected in accordance with the engineering and mechanical properties of the fill material to avoid compromising roadbed stability. However, that study did not specify the indicators used to determine an appropriate energy level. In the present study, by evaluating the deformation modulus following a static load immersion test, it was concluded that a 4,000 kN · m energy level could result in local soil fragmentation, thereby reducing overall stiffness. This finding not only confirmed previous research but also provided a clear evaluative criterion. M. Jia *et al.* (2021b) conducted a numerical investigation using the coupled discrete element-finite difference method. They found that, under continuous impact loading, the soil exhibited a significant lateral compression effect, compacting the soil beyond the radius of the rammer. However, their study did not account for the temporal effects of dynamic compaction. In contrast, in this research, two weeks after the completion of DC treatment, an exploratory well was excavated at the test site, and samples from various depths were collected for laboratory testing. The test results both validated the earlier conclusions and enhanced their applicability to engineering practice. X. Li *et al.* (2024) emphasised that vertical stress distribution should be monitored when determining the reinforcement depth, based on the number of ramming strikes and dynamic stress attenuation, using in-house model tests and numerical simulations. However, their study considered only a single energy level. To address this limitation, the present study conducted multiple tamping tests at four different energy levels and more comprehensively analysed the relationship between tamping energy, number of tamping strikes, and resulting settlement.

J. Zhao *et al.* (2021) investigated the response characteristics of 10,000 kN · m high-energy ramming through numerical simulations and field experiments. They found that effective reinforcement depth initially increases and then stabilises as the number of ramming strikes rises – a conclusion consistent with the findings of the present study under low-energy conditions. W. Zhang *et al.* (2024), through model testing, concluded that a "heavy hammer with low drop spacing" scheme is suitable for loess foundations under wet loading. The results presented in this study are in agreement with their findings. C.J. Lai *et al.* (2020) examined the deformation characteristics of compacted loess under submerged conditions and showed that wetting-induced changes in water content significantly affect soil structural properties. Similarly, the load plate submergence tests on DC-treated soils in this study revealed that water content variation altered the structural characteristics of wetted chalky clay. To understand the roadbed's dynamic response, Y.H. Shang *et al.* (2021) performed excitation tests under both dry and submerged conditions. They found that under identical loads, the dynamic stress at the interface between the roadbed's base and the fill was greater under submerged conditions – a finding corroborated by this study.

H. Bao *et al.* (2024) demonstrated that the interface condition could increase the friction angle while reducing cohesion, leading to an overall decrease in shear strength. The results of this study align with that observation. F. Zhang *et al.* (2025) used geosynthetics to reinforce the cut-and-fill interface and improve slope stability. Building on this, and considering the considerable height and self-weight stress of the fill slope in the current project, a more reliable composite method – "static transition + dynamic reinforcement" – was developed to eliminate the interface effects. L. Zhang *et al.* (2019b) studied the evolution of displacement fields, stress distribution, and plastic zones during DC reinforcement of high-fill embankments using numerical simulations and 2,000 kN · m field tests, determining the optimal number of ramming strikes to be seven. In contrast, the optimum number in the present study was found to be ten, due to the airport project's more stringent requirements regarding foundation settlement and slope stability, and the significantly greater slope height. Consequently, construction parameters, including compaction, required tighter control.

Conclusions

Based on the research experience of a typical high-fill project in China, this study integrated the geotechnical and geological characteristics of an airport site, selected a representative test section with a fill height of nearly 60 metres, and conducted systematic research on the reinforcement of the weak zone at the cut-and-fill interface using the dynamic compaction method. The following conclusions were drawn: the DC tests revealed that single-blow tamping settlement initially increases and then decreases, with the maximum value occurring at the beginning. The settlement per blow tends to decline after 6 to 8 strikes. The cumulative tamping settlement increased with the number of blows. A sharp rise in settlement was observed during the first 3-4 strikes, after which the curve gradually converged from the 10^{th} strike onwards. According to the comprehensive tamping test results, the powdery clay layer was classified as moderately compressible soil. At energy levels of 2,000 kN · m, 3,000 kN · m, and 4,000 kN · m, the optimal number of tamping blows was 11-12, 1214, and 15-16, respectively. The stopping criteria were defined as an average settlement of the final three tamping blows not exceeding 4.5 cm, 5 cm, 5 cm and 7 cm, respectively.

The results of the parallel static load immersion tests showed that post-tamping additional settlement ranged between 11.19 mm and 14.98 mm. The deformation modulus at the 3,000 kN · m energy level was found to be slightly higher than at 4,000 kN · m, due to excessive energy causing localised crushing of the soil, thereby reducing its overall stiffness. Accordingly, the optimal tamping energy for this project was determined to be 3,000 kN · m.

A composite treatment methodology was developed, based on the dual mechanism of "static transition + dynamic enhancement". Key implementations included: constructing 1-4 m high steps at cut-and-fill interfaces; applying three rows of low-energy compaction for every 4 m of fill height at the interface; and reinforcing a zone extending 3 m beyond the slope toe using low-energy dynamic compaction. This approach effectively ensured the quality of soft foundation treatment at interfaces, significantly reduced post-construction settlement of high-fill slopes, and mitigated differential settlement at the cut-and-fill junction.

Acknowledgements

None.

Funding

None.

Conflict of Interest

None.

References

[1] Bao, H., Song, Z., Lan, H., Ma, Y., Yan, C., & Liu, S. (2024). Analysis of the mechanical effects and influencing factors of cut-fill interface within loess subgrade. *Engineering Failure Analysis*, 163, article number 108488. doi: 10.1016/j.engfailanal.2024.108488.

[2] Consoli, N.C., Giese, D.N., Scheuermann Filho, H.C., Festugato, L., Rocha, M.M., Heineck, K.S., & Moreira, E.B. (2020). On porous bonded residual soil in natural and dynamically compacted states through plate load tests. *Journal of Geotechnical and Geoenvironmental Engineering*, 146(8). doi: 10.1061/(ASCE)GT.1943-5606.0002321.

[3] Dawson, E.M., & Roth, W.H. (2020). Slope stability analysis with FLAC. In C. Detournay & R. Hart (Eds.), *FLAC and numerical modeling in geomechanics* (pp. 3-9). London: CRC Press. doi: 10.1201/9781003078531.

[4] GB 50021-2001 (2009). (2002). *Code for investigation of geotechnical engineering*. Retrieved from https://www.codeofchina.com/standard/GB50021-2001(2009).html.

[5] GB 50025-2018. (2018). *Standard for building construction in collapsible loess regions*. Retrieved from https://www.codeofchina.com/standard/GB50025-2018.html.

[6] GB 55003-2021. (2021). *Code for design of building foundation*. Retrieved from https://www.chinesestandard.net/PDF.aspx/GB55003-2021.

[7] GB/T 50123-2019. (2019). *Standard for geotechnical testing method*. Retrieved from https://codeofchina.com/standard/GBT50123-2019.html.

[8] Jia, M., Cheng, J., Liu, B., & Ma, G. (2021a). Model tests of the influence of ground water level on dynamic compaction. *Bulletin of Engineering Geology and the Environment*, 80, 3065-3078. doi: 10.1007/s10064-021-02110-y.

[9] Jia, M., Yang, Y., Liu, B., & Wu, S. (2021b). Densification mechanism of granular soil under dynamic compaction of proceeding impacts. *Granular Matter*, 23, article number 72. doi: 10.1007/s10035-021-01136-z.

[10] Lai, C.J., Zhu, Y.P., & Guo, N. (2020). Water immersion deformation of unsaturated and compacted loess. *Soil Mechanics and Foundation Engineering*, 57, 110-116. doi: 10.1007/s11204-020-09645-4.

[11] Li, P., Sun, J., Ge, X., Zhang, M., & Wang, J. (2023). Parameters of dynamic compaction based on model test. *Soil Dynamics and Earthquake Engineering*, 168, article number 107853. doi: 10.1016/j.soildyn.2023.107853.

[12] Li, X., Lu, Y., Cui, Y., Qian, G., Zhang, J., & Wang, H. (2024). Experimental investigation into the effects of tamper weight and drop distance on dynamic soil compaction. *Acta Geotechnica*, 19, 2563-2578. doi: 10.1007/s11440-023-02198-4.

[13] Li, X., Zhang, K., Ma, X., Teng, J., & Zhang, S. (2020). New method to evaluate strengthen efficiency by dynamic compaction. *International Journal of Geomechanics*, 20(4). doi: 10.1061/(ASCE)GM.1943-5622.0001586.

[14] Li, Y., Fang, Y., & Yang, Z. (2023). Two criteria for effective improvement depth of sand foundation under dynamic compaction using discrete element method. *Computational Particle Mechanics*, 10, 397-404. doi: 10.1007/s40571-022-00506-5.

[15] Mei, Y., Zhang, S., Hu, C., Wang, X., Yuan, Y., Zhao, L., & Zhou, D. (2021). Field test study on dynamic compaction in treatment of a deep collapsible loess foundation. *Bulletin of Engineering Geology and the Environment*, 80, 8059-8073. doi: 10.1007/s10064-021-02343-x.

[16] Ni, W., Nie, Y., Lü, X., & Fan, M. (2024). Mechanical behavior and microstructure evolution of Malan loess under dynamic compaction. *Environmental Earth Sciences*, 83(2), article number 76. doi:10.1007/s12665-023-11361-9.

[17] Shang, Y. H., Xu, L. R., & Cai, Y. (2021). Study on dynamic characteristics of cement-stabilized expansive soil subgrade of heavy-haul railway under immersed environment. *Rock and Soil Mechanics*, 41(8). doi: 10.16285/j.rsm.2019.6467.

[18] Sun, Y., Huang, K., Chen, X., Zhang, D., Lou, X., Huang, Z., Han, K., & Wu, Q. (2023). Study on the reinforcement mechanism of high-energy-level dynamic compaction based on FDM–DEM coupling. *Mathematics*, 11(13), article number 2807. doi: 10.3390/math11132807.

[19] Wang, L., Du, F., Liang, Y., Gao, W., Zhang, G., Sheng, Z., & Chen, X. (2023). A comprehensive in situ investigation on the reinforcement of high-filled red soil using the dynamic compaction method. *Sustainability*, 15(6), article number 4756. doi: 10.3390/su15064756.

[20] Wu, S., Wei, Y., Zhang, Y., Cai, H., Du, J., Wang, D., Yan, J., & Xiao, J. (2020). Dynamic compaction of a thick soil-stone fill: Dynamic response and strengthening mechanisms. *Soil Dynamics and Earthquake Engineering*, 129, article number 105944. doi: 10.1016/j.soildyn.2019.105944.

[21] Xi, L., Xun. Z., Xinyan, M., & Sheng, Z. (2020). Three-dimensional simulation of dynamic compaction for earth-rock fill by discrete element method. *Journal of Beijing Jiaotong University*, 44(3), article number 88. doi: 10.11860/j.issn.1673-0291.20190002.

[22] Yao, Z., Zhou, C., Lin, Q., Yao, K., Satchithananthan, U., Lee, F.H., Tang, A.M., Jiang, Y., Pan, Y., & Wang, S. (2022). Effect of dynamic compaction by multi-point tamping on the densification of sandy soil. *Computers and Geotechnics*, 151, article number 104949. doi: 10.1016/j.compgeo.2022.104949.

[23] Zhang, F., Jia, S., & Gao, Y. (2025). Stability analysis of cut-fill and deep patch unsaturated slopes under steady infiltration conditions. *Science China Technological Sciences*, 68(1), article number 1120701. doi: 10.1007/s11431-024-2800-8.

[24] Zhang, L., Yang, G., Zhang, D., Hou, L., & Jin, J. (2019a). Research on the mechanism and testing technology of dynamic compaction of high-filled gravel soil roadbed. *IOP Conference Series: Earth and Environmental Science*, 304(3), article number 032097. doi: 10.1088/1755-1315/304/3/032097.

[25] Zhang, L., Yang, G., Zhang, D., Wang, Z., & Jin, J. (2019b). Field test and numerical simulation of dynamic compaction of high embankment filled with soil-rock. *Advances in Civil Engineering*, 2019(1), article number 6040793. doi: 10.1155/2019/6040793.

[26] Zhang, W., Mu, H., Liu, F., Guo, H., Zhao, W., & Xue, Y. (2024). Physical model tests on reinforced loess foundation model under wetting and loading. *Journal of Engineering Science and Technology*, 17(3). doi: 10.12454/j.jsuese.202400249.

[27] Zhao, J., Lü, J., Zhao, H., Sun, H. (2021). Effective reinforcement depth of high energy dynamic compaction for filled subgrade. *Journal of Civil and Environmental Engineering*, 43(5), 27-33. doi: 10.11835/j.issn.2096-6717.2020.091.

[28] Zhou, W.H., & Yin, Z.Y. (2022). *Practice of discrete element method in soil-structure interface modelling*. Singapore: Springer. doi:10.1007/978-981-19-0047-1.

[29] Zhu, J., Zheng, J., Yu, Y., Dong, B., Wang, Y., & Zhang, W. (2025). Neural network modeling and sensitivity analysis of factors influencing dynamic compaction vibration velocity. *Periodica Polytechnica Civil Engineering*, 69(2), 664-675. doi: 10.3311/PPci.37967.

Аэропортто жайгашкан бийик насыя фундаменттердин жер алдындагы катмар менен насыянын чек арасы болгон интерфейсинде динамикалык тыгыздоону армировка жолу менен колдонуу боюнча изилдөө

Чен Сяобин
Аспирант
Винница улуттук техникалык университети
21021, Хмельницкое шоссе көч., 95, Винница шаары, Украина
Магистр
Цзюцюань кесиптик технологиялар институту
735000, 66 Цзефан шоссе, Цзюцюань шаары, Кытай
https://orcid.org/0009-0002-9675-6410

Вячеслав Джеджула
Экономика илимдеринин доктору, профессор
Винница улуттук техникалык университети
21021, Хмельницкое шоссе көч., 95, Винница шаары, Украина
https://orcid.org/0000-0002-2740-0771

Аннотация. Кытайда айдоо жерлери катуу корголгондуктан, «тоолорду казып, арыктарды толтуруунун» бийик толуп жаткан долбоорлору кебейуп жатат. Жер астындагы катмардын үстүн туура эмес иштетүү инженердик кырсыктарга, мисалы, тегиз эмес отурукташууга жана эңкейиштин туруксуздугуна алып келиши мүмкүн. Бул эмгектин максаты жээктеги топурактардын динамикалык тыгыздалуу механизмин жана суу чөйрөсүнүн өзгөрүшүнүн тыгыздалуу таасирине тийгизген таасирин ачып берүү жана казуу менен жээк тилкелеринин ортосундагы алсыз интерфейстердин көйгөйүн чечүү үчүн инженердик чараларды илимий жактан негиздөө болгон. Кытайдын түндүк-батышындагы тоолуу аймактагы трафик көп болгон аэропорттун долбоорунун негизинде талаанын динамикалык тыгыздалуу сыноолору, түпкү фундаменталдык топурактын статикалык жүккө чөмүлүү сыноолору, ички геотехникалык сыноолор жүргүзүлдү жана FLAC3D сандык моделинин негизинде күчөтүлгөн жантаймалардын коопсуздук коэффициенти эсептелди. Изилдөөнүн натыйжалары көрсөткөндөй: бир жолку тампингдин отурушу энергиянын көбөйүшү менен көбөйөт жана тактоо убактысынын көбөйүшү менен азаят; отурукташуу 3-4 жолу таптап баштаганда эң чоң болуп, 6-8 жолу таптагандан кийин акырындап турукташат; Тыюулангандан кийин кыртыштын кургак тыгыздыгы жана ийкемдүү модулу жогорулаган, өсүү мааниси таптап чыгуу энергиясы менен оң корреляцияланган жана үлгү алуу тереңдигинин өсүшү менен акырындык менен азайган. Туруктуу токтун зонасында статикалык жүктү чөмүлүү сынагынын жыйынтыгы көрсөткөндөй, чөмүлүү ныкталган топурактын кошумча отурушун шарттайт, ал эми ныктоо учурунда тампинг энергиясы канчалык жогору болсо, чөмүлүүдөн кийин кошумча отуруунун көлөмү ошончолук аз болот. Бул эмгектин натыйжалары туруктуу токтун параметрлерин долбоорлоо жана казуунун жана жээктин тилкесиндеги жумшак зонанын көйгөйлөрүн чечүү үчүн инженердик иш-чаралардын негизин түзөт

Негизги сөздөр: тоо-кен инженериясы; статикалык сууга чөмүлүү сыноо; алсыз катмарды бекемдөө; интерфейсти бекемдөө ыкмасы; FLAC3D сандык симуляциясы